Thermal properties, crystal structures, and phase diagrams of ionic plastic crystals and ionic liquids containing a chiral cationic sandwich complex

Mochida, Tomoyuki
Sumitani, Ryo
Yamazoe, Tomoaki

PAPER

Thermal Properties, Crystal Structures, and Phase Diagrams of Ionic Plastic Crystals and Ionic Liquids Containing a Chiral Cationic Sandwich Complex†

Received 00th January 20xx,
Accepted 00th January 20xx

DOI: 10.1039/x0xx00000x

Tomoyuki Mochida,*[a,b] Ryo Sumitani [a] and Tomoaki Yamazoe [a]

To investigate the effects of chirality on the phase behavior of ionic plastic crystals and ionic liquids, salts of a chiral sandwich complex with various anions were synthesized. The synthesized salts have the general chemical formula, $[Ru(C_5H_5)(C_6H_5CHCH_3OCH_3)]X$ (X = $CB_{11}H_{12}$, CF_3BF_3, PF_6, CPFSA (= $CF_2(SO_2CF_2)_2N$)), where the ruthenium complex possesses a chiral substituent. The racemates of the salts with the $CB_{11}H_{12}$, CF_3BF_3, and PF_6 anions crystallized as a solid solution, racemic compound, and conglomerate, respectively. The (*S*)-enantiomer and the racemate of the $CB_{11}H_{12}$ salt exhibited phase transitions to the ionic plastic phase and melted at high temperatures. Further, this salt exhibited polymorphism, as crystallographically investigated. Most of the other salts were ionic liquids exhibiting no plastic phase. The CPFSA salt was liquid and exhibited glass transition at low temperatures.

Introduction

In recent years, extensive studies have been conducted on ionic plastic crystals (IPCs) and ionic liquids (ILs). IPCs are solids that consist of globular molecules, where the constituent molecules exhibit orientational disorder owing to rapid rotation.[1-6] Plastic crystals generally display a small entropy of fusion as a consequence of the disorder (ΔS < 20 $JK^{-1}mol^{-1}$), and they exhibit highly symmetric crystal lattices such as cubic or hexagonal. Various onium salts exhibit a plastic phase with high ionic conductivity, and their phase transition behavior and electronic properties have attracted significant interest.[5-10] In contrast, ILs are salts with melting points below 100 °C. ILs have attracted considerable interest for their application as solvents and in electrochemistry owing to their characteristic properties such as nonvolatility, nonflammability, and high ionic conductivity.[11] Recently, we developed a variety of IPCs[12-16] and ILs[17-21] containing cationic sandwich complexes. The plastic phase is ascribed to the globular shape of the sandwich complexes.[22,23] The use of organometallic complexes for IPCs or ILs leads to various functions such as magnetic properties,[15-18] electrical properties,[19] and photochemical reactivities,[20,21] which are not exhibited by onium salts. To elucidate the boundary between IPCs and ILs, we previously investigated the phase behavior of sandwich complex salts, which is shown in Fig. 1 (R = H, Me, Et, ^{n}Bu; X = PF_6, $B(CN)_4$, $(FSO_2)_2N$).[24] The salts with R = H and Me exhibited IPC phases at high temperatures, whereas those with R = Et and ^{n}Bu were mostly ILs. These studies also revealed the anion dependence of the phase-transition temperatures, as in the case of onium salts.[25]

Understanding the effect of chirality on the structures and physical properties of molecular solids is essential in crystal engineering and pharmaceutical science.[26] A racemate crystallizes either as a racemic compound, conglomerate, or solid solution.[26-30] A racemic compound contains equal amounts of (*S*)- and (*R*)-enantiomers arranged uniformly in a crystal, whereas a conglomerate is a physical mixture of enantiopure crystals. Approximately 90% of organic racemate crystals form racemic compounds, while most of the rest form conglomerates; in contrast, solid solutions are rarely formed.[26] Thus far, many chiral ILs have been synthesized owing to their applications in asymmetric syntheses, and so forth.[31-34] We investigated the effect of chirality on the thermal properties of ILs, using organometallic ILs with chiral long-chain substituents, and revealed that the racemate tends to exhibit low crystallinity and a lower melting point than that of the enantiomer.[35,36] In contrast, the effect of chirality on the thermal properties of IPCs has not been elucidated, though IPCs containing a chiral quaternary ammonium cation have been reported.[37,38] Comparative thermal studies involving racemates have been conducted on neutral chiral plastic crystals such as camphor.[26,39]

The purpose of this study is to investigate the effect of chirality on the phase behavior of IPCs and ILs. For this purpose, salts of a cationic ruthenium sandwich complex with a chiral substituent were synthesized, and the phase behaviors of their

[a] *Department of Chemistry, Graduate School of Science, Kobe University, 1-1 Rokkodai, Nada, Kobe, Hyogo 657-8501, Japan. E-mail: tmochida@platinum.kobe-u.ac.jp*
[b] *Center for Membrane Technology, Kobe University, 1-1 Rokkodai, Nada, Kobe, Hyogo 657-8501, Japan*

† Electronic supplementary information (ESI) available: DSC traces (Figs. S1 and S2), PXRD patterns (Figs. S3 and S4), 1H NMR spectrum (Fig. S5), and crystallographic parameters (Table S1). CCDC 2027267 (*rac*-[**1**]$CB_{11}H_{12}$, α-form), 2023096 (*rac*-[**1**]$CB_{11}H_{12}$, β-form), and 1991383 ((*S*)-[**1**]PF_6). For ESI and crystallographic data in CIF or other electronic format see DOI: 10.1039

(*S*)-enantiomers and racemates were examined ((*S*)-[**1**]X and *rac*-[**1**]X, Fig. 2a). The $CB_{11}H_{12}$ (monocarba-*closo*-dodecarborate), CF_3BF_3, PF_6, and CPFSA (= $CF_2(SO_2CF_2)_2N$) anions were employed as the counter anions (Fig. 2b). These globular anions were chosen to investigate the phase behavior of IPCs. The $CB_{11}H_{12}$ anion is a stable, weakly coordinating carborane anion with an icosahedral geometry suitable for IPCs.[40] Other anions also yield organometallic IPCs.[12,14] However, in this study, only the $CB_{11}H_{12}$ salt exhibited a plastic phase, and most of the other salts were ILs. The examination of their phase behaviors revealed that the racemate crystal forms in these salts varied between a solid solution, racemic compound, and conglomerate, depending on the anion.

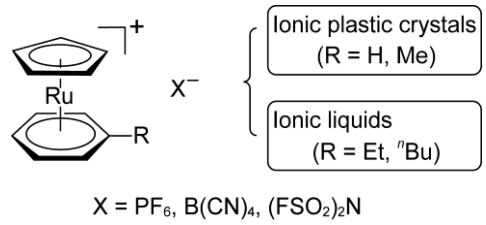

Fig. 1 Molecular structures and phase behaviors of some salts of cationic ruthenium sandwich complexes.

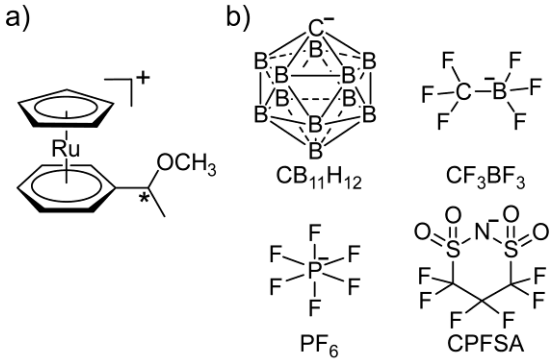

Fig. 2 Structures of the (a) cation and (b) anions used in this study. The asterisk in (a) indicates the chiral center.

Results and discussion

Phase behavior

(*S*)-[**1**]PF_6 was synthesized by the reaction of [Ru(C_5H_5)($NCCH_3$)$_3$]PF_6 and (*S*)-$PhCHCH_3OCH_3$, whereas the other salts were obtained via anion exchange with the PF_6 salt. The corresponding racemates were synthesized using a racemic ligand. The thermal properties of the synthesized salts were investigated by differential scanning calorimetry (DSC). The melting points and classification of the salts are summarized in Table 1. The $CB_{11}H_{12}$ salts exhibited a plastic phase at high temperatures, whereas the other salts were mostly ILs with no plastic phase. It is to be noted that these salts possessed different racemate crystal forms depending on the anions, as listed in Table 1. The CPFSA salt was liquid and exhibited glass transition at low temperatures.

The phase sequences of the (*S*)-enantiomer and the racemate of the salts, except the CPFSA salt, are shown in Fig. 3. The $CB_{11}H_{12}$ salt possessed polymorphic forms, among which the dominant form (α-form) was thermally characterized. This salt underwent successive phase transitions from phase III to II, and subsequently to I* (plastic phase). Such two-step phase transitions are often observed in IPCs containing sandwich complexes, owing to the disorder of anions and cations exhibited at different temperatures.[18] The phase transition temperatures to the plastic phase for the (*S*)-enantiomer and racemate were 66.4 and 80.3 °C, respectively, and they melted at almost the same temperature: 259.5 and 251.3 °C, respectively. Their melting entropies were less than 20 J mol^{-1} K^{-1}, which is characteristic to the plastic phase.[41,42] The disappearance of birefringence in the plastic phase was also confirmed by polarizing microscopic observation. It is to be noted that the transition temperatures to the plastic phase were much lower than those of unsubstituted sandwich complexes with the same anion, such as [Ru(C_5H_5)(C_6H_6)]$CB_{11}H_{12}$ (T_C = 228 °C) and [Co(C_5H_5)$_2$]$CB_{11}H_{12}$ (T_C = 129 °C).[12] The relatively low transition temperatures for less-symmetrical cations have been observed in other organometallic salts.[12,13]

The salts with the other anions had much lower melting points, most of which were below 100 °C. The melting points of the (*S*)-enantiomer and the racemate of the CF_3BF_3 salt were 37.1 and 12 °C, respectively. The melting points of the corresponding PF_6 salts were 105.0 and 70.0 °C, respectively. The higher melting points of the PF_6 salts than those of the CF_3BF_3 salts are ascribed to the smaller anion size of the former. The melting point of the racemate was lower than that of the enantiomer in each salt. The melting entropies of these salts ranged from 50 to 82 J mol^{-1} K^{-1}. In contrast, the CPFSA salts

Table 1 Melting points (°C) and classification of the salts prepared in this study[a]

	melting point (°C)			
	[**1**]$CB_{11}H_{12}$ (α-form)	[**1**]CF_3BF_3	[**1**]PF_6	[**1**]CPFSA
(*S*)-enantiomer	259.5 (IPC)	37.1 (IL)	105.0	−55[c]
Racemate	251.3 (IPC)	12[b] (IL)	70.0 (IL)	−55[c]
	solid solution[d]	racemic compound[d]	conglomerate[d]	

[a]IPC: ionic plastic crystal, IL: ionic liquid. [b]Not precise due to successive phase transitions. [c]Glass transition temperature. [d]Type of racemate crystal.

were liquid at ambient temperature, with a glass transition temperature of –55 °C. The (*S*)-enantiomer, racemate, and the 50% ee sample of the salt exhibited glass transition at the same temperature (Fig. S1, ESI†), which is rational because the enantiomers are structurally similar.

The salts of unsubstituted sandwich complexes, such as $[Ru(C_5H_5)(C_6H_6)]X$ and $[Co(C_5H_5)_2]X$ (X = CF_3BF_3 and PF_6), exhibit plastic phases.[12,23] However, here, only the $CB_{11}H_{12}$ salt containing a bulky spherical anion exhibited a plastic phase. This is probably because the other salts possessed low melting points and melted before exhibiting the plastic phase. The following sections explain the thermal properties and crystal structures of the solid salts.

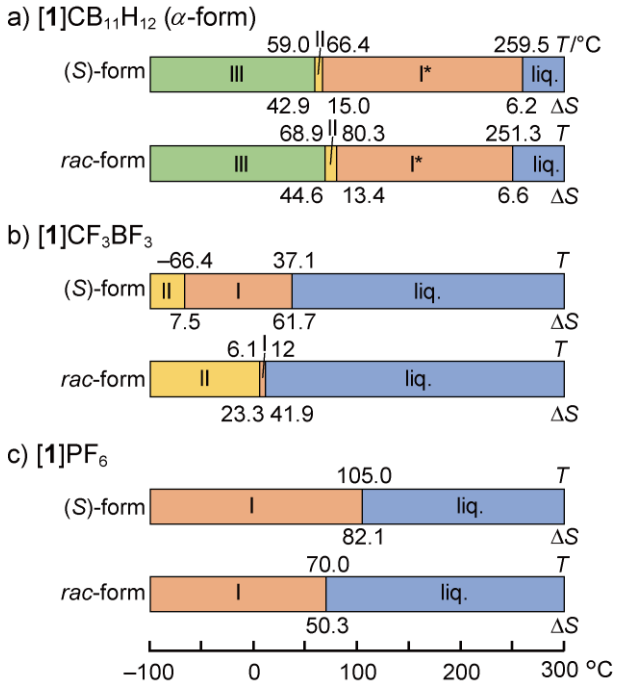

Fig. 3 Phase diagrams of (*S*)-[**1**]X and *rac*-[**1**]X [X = $CB_{11}H_{12}$ (*α*-form), CF_3BF_3, PF_6]. The phase-transition temperatures (°C) and phase-transition entropies (J mol^{-1} K^{-1}) are shown above and below each bar chart, respectively, where liq. indicates the liquid phase. The decomposition temperatures are not considered in the diagram.

Phase behavior of the $CB_{11}H_{12}$ salt

The thermal properties of the *α*-form of the $CB_{11}H_{12}$ salt were investigated, and revealed successive phase transitions to yield the plastic phase. The enantiomers form solid solutions in the solid state.

The DSC traces of (*S*)- and *rac*-[**1**]$CB_{11}H_{12}$ are shown in Fig. 4. Upon heating, the (*S*)-enantiomer exhibited phase transitions from phase III to II at 59.0 °C (ΔS = 42.9 J mol^{-1} K^{-1}) and phase II to I* (plastic phase) at 66.4 °C (ΔS = 15.0 J mol^{-1} K^{-1}). The racemate exhibited a similar phase sequence at a slightly higher transition temperature: from phase III to II at 68.9 °C (ΔS = 44.6 J mol^{-1} K^{-1}) and thereafter to phase I* at 80.3 °C (ΔS = 13.4 J mol^{-1} K^{-1}). A solid with an intermediate enantiomeric excess exhibited phase-transition peaks between those of the (*S*)-enantiomer and the racemate (Fig. 4, inset). In addition, powder X-ray diffraction (PXRD) patterns of the solids at ambient temperature were identical regardless of the enantiomeric excess (see below). These results indicate the formation of a solid solution. The higher transition temperature of the racemate to the plastic phase, compared to that of the (*S*)-enantiomer, is possibly ascribed to the denser packing of the molecules in the racemic crystals.[43,44] Upon heating the plastic phase, the (*S*)-enantiomer and racemate melted at 259.5 °C (ΔS_m = 6.2 J mol^{-1} K^{-1}) and 251.3 °C (ΔS_m = 6.6 J mol^{-1} K^{-1}), respectively. Their comparable melting points and melting entropies are consistent with their identical plastic phase structures (see below). It is known that globular chiral molecules that exhibit plastic phases, such as camphor, form solid solutions of enantiomers.[26] Furthermore, IPCs containing globular cations form solid solutions, and their phase-transition temperatures are modulated according to the composition.[2] Therefore, the formation of a solid solution in the current case is reasonable. It is to be noted that the phase transition peaks to the plastic phase in the second and subsequent DSC traces were different from those in the first cycle (Fig. S2, ESI†). This is ascribed to the formation a different crystal structure upon cooling from the plastic phase, as shown below.

The baseline of the DSC trace begins to deviate slightly near the melting point in both cases, indicating the onset of gradual decomposition. Therefore, the thermal stability of the racemate was investigated by thermogravimetric-differential thermal analysis (TG-DTA, at 10 °C min^{-1} under a nitrogen atmosphere). The TG curve shows gradual weight loss above the melting point, exhibiting a one-step weight loss of approximately −10 wt% at approximately 330 °C (Fig. 5). The weight loss corresponded to the elimination of the chiral substituent in the cation (calc. −12 wt %). In the DTA curve, several endothermic peaks consistent with decomposition were observed above the melting point.

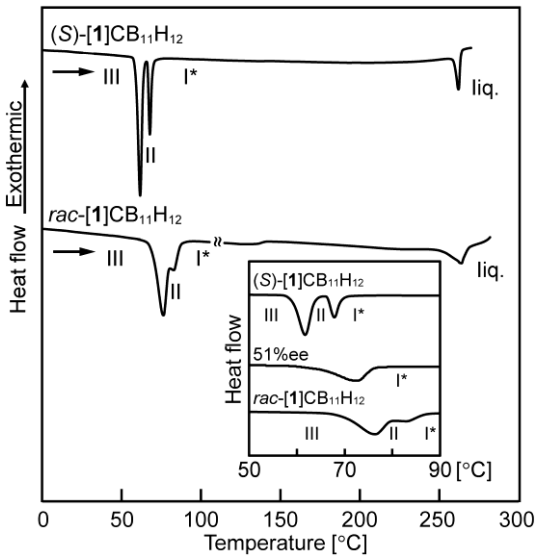

Fig. 4. DSC traces of (*S*)- and *rac*-[**1**]$CB_{11}H_{12}$ recorded on heating runs (10 °C min^{-1}), where liq. represents the liquid state. The trace for the racemic sample above 100 °C was recorded on a subsequent run. The inset shows the magnified view, including the DSC trace of the 51% ee sample.

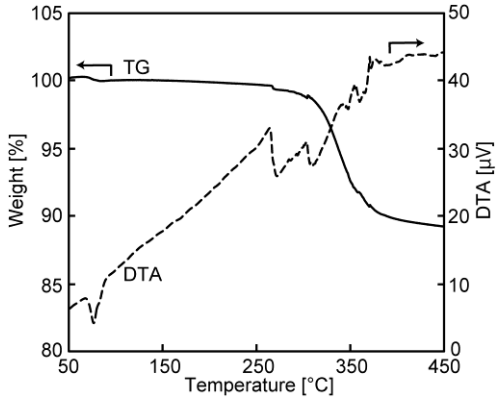

Fig. 5. TG–DTA traces of *rac*-[**1**]$CB_{11}H_{12}$ recorded at 10 °C min^{-1} under a nitrogen atmosphere. The TG and DTA curves are represented by solid and dashed lines, respectively.

Structures of the $CB_{11}H_{12}$ salt

Single-crystal X-ray structure analysis was performed on two polymorphs of *rac*-[**1**]$CB_{11}H_{12}$ at −183°C. The α-form was obtained by bulk recrystallization, whereas the β-form was obtained as a minor component when crystallized by the diffusion method. They crystallized in centrosymmetric space groups $P2_1/c$ and $P\bar{1}$, respectively, exhibiting different packing arrangements. The packing diagrams are shown in Fig. 6. In both crystals, the asymmetric unit contains a cation and anion pair. The orientation of the anion was ordered in both polymorphs, and the B–C and B–B bond lengths were approximately 1.72 Å and 1.78 Å, respectively, which are typical values.[40]

In the α-form (Z = 4), the substituent in the cation exhibited a two-fold disorder with a 0.5:0.5 occupancy. This is a statistical, enantiomeric disorder owing to the coexistence of (*S*)- and (*R*)-enantiomers. Though we could not perform the structure analysis of the (*S*)-enantiomer crystal, the result suggests that the enantiomer, exhibiting an identical PXRD pattern with that of the racemate, crystallizes in a space group $P2_1$ or *Pc*, which are the subgroups of $P2_1/c$.[29] The formation of a solid solution is reasonable considering the enantiomerically disordered crystal structure of the racemate. In contrast, the unit cell of the β-form is half that of the α-form (Z = 2), and there is no disorder in the cation substituent. The crystal contains both enantiomers related by inversion symmetry. Therefore, it can be regarded as a racemic compound, though a solid solution could be also formed in this case.[29]

In both crystals, the cations and anions were arranged alternately, and there were no π–π contacts between the cations. One anion was surrounded by eight cations and vice versa. The van der Waals radii of the cation and anion estimated from the density functional theory (DFT) calculation are 3.90 and 3.49 Å, respectively, and the radius ratio, ρ (= r_{small}/r_{large}), is 0.90. This is consistent with the radius ratio rule of ionic crystals, which predicts the eight-coordinate structure for salts with ρ > 0.73.[45,46]

The plastic phase structure of the salt was further investigated by PXRD measurements at 80 °C. It was revealed that the (*S*)-enantiomer and racemate both possessed a CsCl structure with a lattice constant of a = 8.31 Å (Fig. S3, ESI†). The eight-coordinate structure is consistent with the radius ratio rule. The interionic distance of 7.21 Å calculated from the lattice constant agrees with the sum of the van der Waals radii of cations and anions (7.39 Å). It is to be noted that the PXRD patterns of the solids formed upon cooling the plastic phases were different from either of those of the α- and β-form (Fig. S3, ESI†), suggesting the formation of another polymorph.

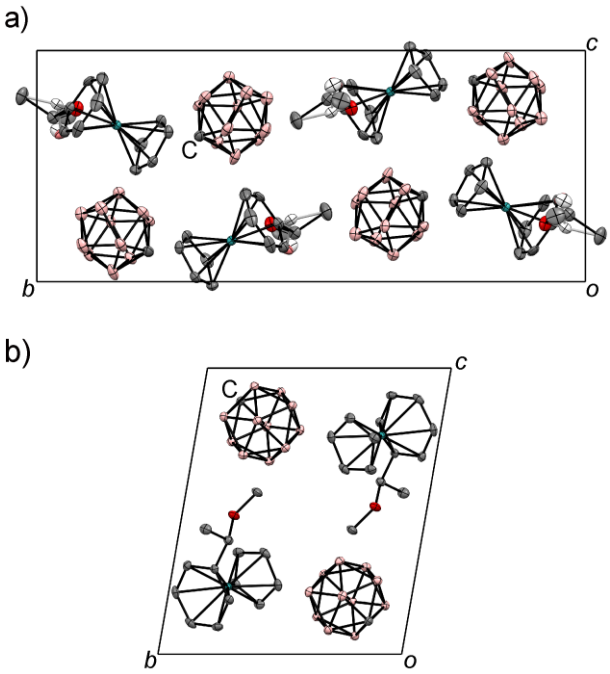

Fig. 6. Packing diagrams of the (a) α- and (b) β- forms of *rac*-[**1**]$CB_{11}H_{12}$ determined at −183 °C. The hydrogen atoms have been omitted for clarity. A part of the disorder of the cation substituent in (a) is displayed in gray.

Phase behavior of the CF_3BF_3 salt

The CF_3BF_3 salt exhibited a typical binary phase diagram of a racemic-compound-forming substance. Consistently, the crystals of the (*S*)-enantiomer and the racemate exhibited different PXRD patterns, demonstrating that the racemate is a racemic compound (Fig. S4a, ESI†).

The DSC traces of the salts with different enantiomeric excesses are shown in Fig. 7a. The (*S*)-enantiomer underwent solid-phase transition from phase II to I at −66.4 °C (ΔS = 7.5 J mol^{-1} K^{-1}) and melted at 37.1 °C (ΔS_m = 61.7 J mol^{-1} K^{-1}) upon heating. In contrast,

the racemate crystals exhibited successive phase transitions at 6.1 and 12 °C (ΔS_{total} = 65 J mol^{-1} K^{-1}). The diffraction patterns were almost unchanged in both phases, which suggests that the phase transition is probably associated with a change in the molecular motion. Upon cooling from the liquid state, the (*S*)-enantiomer exhibited only crystallization, but the racemate exhibited partial crystallization and the remaining liquid exhibited glass transition at –78 °C. The ratio of the glass transition temperature to the melting point in the racemate was 0.68, which agrees with the empirical rule, T_g/T_m = 2/3, that holds for molecular materials.[47,48]

The solid-liquid phase diagram of the salts as a function of the enantiomeric excess is shown in Fig. 7b. The peak top temperatures in the DSC traces were used to plot the data. The phase diagram is typical for a racemic compound, where the sample with 50% ee possesses a eutectic composition. The liquidus lines of racemic compounds are theoretically expressed using the Schröder–van Laar equation at % ee > 50% and the Prigogine–Defay equation at % ee < 50%, using the enthalpy of fusion and melting points of the enantiomer and the racemate.[26] The observed phase behavior agrees with the theoretical liquidus lines shown in the phase diagram. The deviation from the theoretical line may be due to the broadness of the melting peaks. The melting point of a racemic compound can be higher or lower than that of the enantiomer;[26] here, the racemic compound showed a lower melting point than that of the (*S*)-enantiomer.

Phase behavior of the PF_6 salt

The PF_6 salt exhibited a typical binary phase diagram of a conglomerate-forming substance. Consistently, the crystals of the (*S*)-enantiomer and the racemate exhibited the same PXRD patterns, confirming that the racemate crystallized as a conglomerate (Fig. S4b, ESI†); this is further verified by the crystal structure analysis.

The DSC traces of the salts with different enantiomeric excesses are shown in Fig. 8a. The melting points of the (*S*)-enantiomer and the racemate of the PF_6 salt were 105.0 °C (ΔS_m = 82.1 J mol^{-1} K^{-1}) and 70.0 °C (ΔS_m = 50.3 J mol^{-1} K^{-1}), respectively. The samples with intermediate enantiomeric excess exhibited melting peaks at temperatures between the melting points of the (*S*)-enantiomers and those of the racemates. The eutectic melting peaks were also observed. The solid–liquid phase diagram, as a function of the enantiomeric excess, is shown in Fig. 8b. The racemate, possessing a eutectic composition, has a lower melting point than that of the (*S*)-enantiomer, which is typical for a conglomerate-forming substance.[26] The liquidus line, drawn using the Schröder–van Laar equation, is consistent with the observed melting points.[26] The mixing enthalpy calculated from the melting points and melting enthalpies of the enantiomer and racemate was ΔS = 6.4 mol^{-1} K^{-1}, which is a reasonable value comparable to R ln 2 (5.76 mol^{-1} K^{-1}).[49]

The single crystals were subjected to the X-ray structure analysis, and the packing diagram of (*S*)-[**1**]PF_6 is shown in Fig. 9. The enantiomer crystallized in the chiral space group, $P2_12_12_1$ (Z = 4). The asymmetric unit contains a cation and anion pair. The cations and anions were arranged alternately in the crystal, and there were no π–π contacts between the cations. In contrast, the racemic crystals were found to be inverted twins consisting of (*S*)- and (*R*)-crystals, demonstrating that the racemate crystallized as a conglomerate. These results are consistent with those of the PXRD experiments mentioned above.

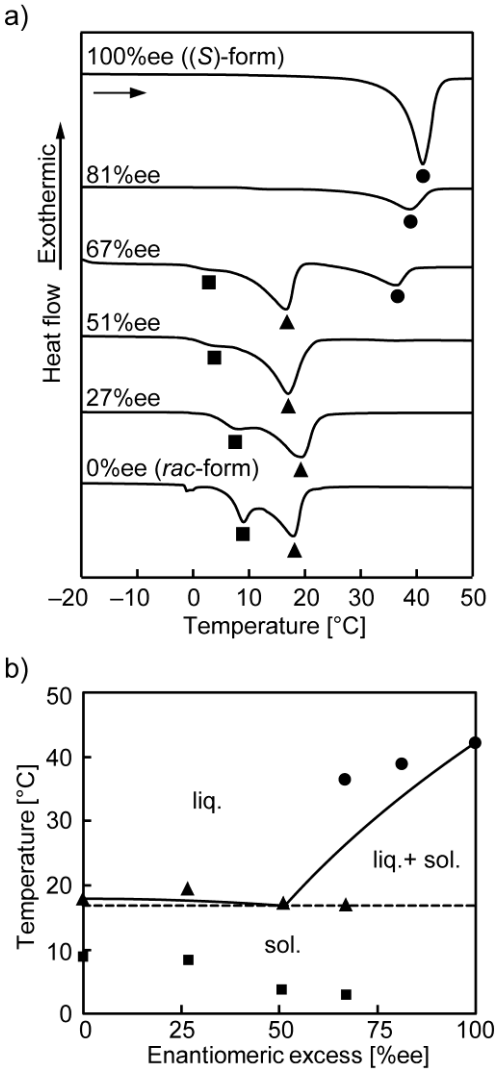

Fig. 7. (a) DSC traces and (b) solid–liquid phase diagram of [**1**]CF_3BF_3 with different enantiomeric excesses. The symbols correspond to the melting of the (*S*)-enantiomer (●), racemate and eutectic mixtures (▲), and solid-phase transition (■). Liq. and sol. represent the liquid and solid states, respectively. The solid line is the liquidus line drawn using the Schröder–van Laar (%ee > 50%) and Prigogine–Defay (%ee < 50%) equations, and the dotted line represents the eutectic point.

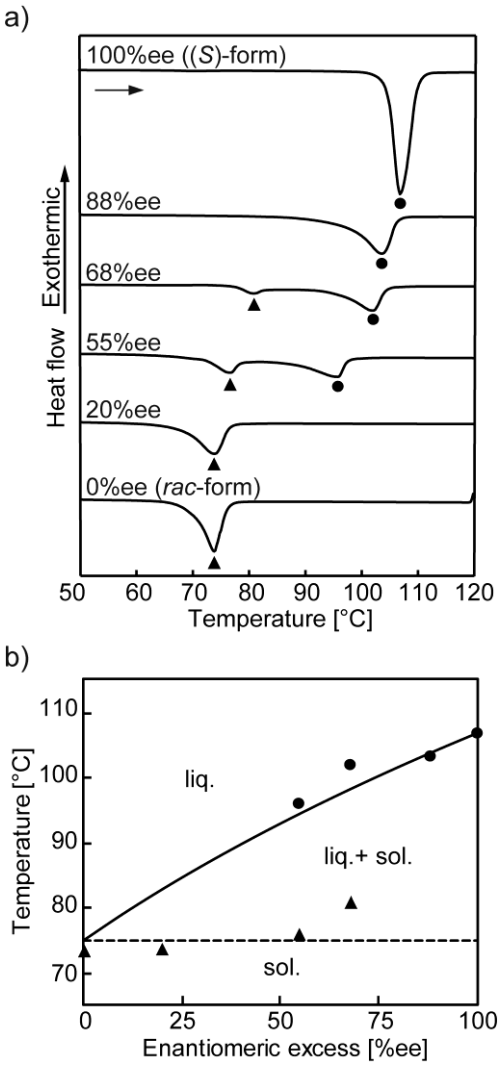

Fig. 8. (a) DSC traces and (b) solid–liquid phase diagram of [**1**] PF_6 with different enantiomeric excesses, where liq. and sol. are the liquid and solid states, respectively. The symbols correspond to the melting of the (*S*)-enantiomer (●), as well as the racemate and eutectic mixture (▲). The solid line is the liquidus line drawn using the Schröder-van Laar equation, and the dotted line indicates the eutectic point.

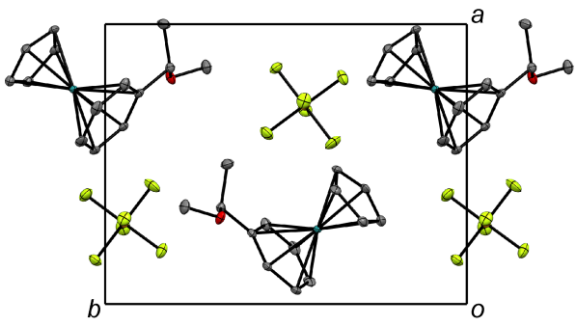

Fig. 9. Packing diagram of (*S*)-[**1**]PF_6 determined at −183 °C. The hydrogen atoms have been omitted for clarity.

Conclusions

The salts of a cationic chiral ruthenium sandwich complex with various anions were synthesized. Although the salts of cationic unsubstituted sandwich complexes often exhibit a plastic phase, only the $CB_{11}H_{12}$ salt in the current study exhibited a plastic phase, and most of the other salts were ILs. Furthermore, the racemate crystal forms were dependent on the anion, and the racemates of the $CB_{11}H_{12}$, BF_3CF_3, and PF_6 salts crystallized as a solid solution, racemic compound, and conglomerate, respectively. The $CB_{11}H_{12}$ salt had polymorphic forms, of which the dominant form exhibited an enantiomeric disorder in the racemate crystal. The characteristic features of the $CB_{11}H_{12}$ salt are ascribed to the globular molecular shapes of the cation and anion. It is known that globular chiral molecules (such as camphor) that exhibit the plastic phase form solid solutions, though there have been no such investigations on chiral IPCs. The structures and thermal properties of IPCs and the glass transition temperature of ILs in the current salts hardly depend on chirality, which is reasonable from the viewpoint of symmetry. The results are useful for material design and the applications of IPCs and ILs. In particular, organometallic IPSc and ILs exhibit various functions, hence the control of their thermal properties through chirality control may be useful for their future applications.

Experimental

General

Cesium carborane ($CsCB_{11}H_{12}$), potassium (trifluoromethyl)trifluoroborate (KCF_3BF_3, > 95%), and lithium 1,1,2,2,3,3,-hexafluoropropane-1,3-disulfonamide (LiCPFSA, > 98%) were purchased from Strem Chemicals, Indofine chemical, and Tokyo Chemical Industry, respectively. $[Ru(C_5H_5)(NCCH_3)_3]PF_6$ and (*S*)-$C_6H_5CHCH_3OCH_3$ were prepared following previously reported procedures.[50,51] ^1H and ^{19}F NMR spectra were recorded on a Bruker Avance 400 MHz spectrometer. TG–DTA analyses were performed under a nitrogen atmosphere at a heating rate of 10 °C min^{-1} on a Rigaku TG8120 thermogravimetric analyzer. An aluminum pan was used as the sample container. DSC measurements were performed on a TA instrument Q100 differential scanning calorimeter at a scan rate of 10 °C min^{-1} using aluminum hermetic pans as the sample containers. The sample with intermediate enantiomeric excess was prepared by dissolving the mixture of the (*S*)-enantiomer and the racemate in dichloromethane, after which the solvent was evaporated. The residue was dried under vacuum at 60 °C for 2 h, and then subjected to freeze, pump, and thaw cycles for the complete removal of the solvents. The samples were heated above the melting point for 5 min prior to the measurements to ensure uniform mixing. The temperature dependence of the PXRD measurements was investigated using a Bruker APEX II Ultra (MoKα). The radii of the cations and anions were calculated by assuming spheres of the same molecular volume, as determined by DFT calculations.[12] Calculations were performed at the ωB97-D/LanL2DZ level using Spartan '18 software (Wavefunction Inc.).

Preparation of $[Ru(C_5H_5)((S)\text{-}C_6H_5CHCH_3OCH_3)]PF_6$ ((*S*)-[1]PF_6)

(*S*)-$C_6H_5CHCH_3OCH_3$ (0.023 mL, 0.15 mmol) was added to a 1,2-dichloroethane solution (0.6 mL) of $[Ru(C_5H_5)(NCCH_3)_3]PF_6$ (50 mg, 0.12 mmol), and the resulting solution was stirred at 90 °C for 18 h under a nitrogen atmosphere. Thereafter, the solvent was evaporated under reduced pressure and dried under vacuum at 60 °C for 2 h. The residue was dissolved in dichloromethane and charged into a short column of alumina. Impurities were first eluted with dichloromethane, following which the desired product was eluted with acetonitrile. The product was recrystallized from diethyl ether/dichloromethane at −40 °C. Pale yellow crystals (39 mg, yield 72%) were obtained. ^{1}H NMR (400 MHz, $CDCl_3$): δ = 1.41 (d, 3H, *J* = 6.44 Hz, –CH*CH*$_3$), 3.40 (s, 3H, –O*CH*$_3$), 4.30 (q, 1H, *J* = 6.4 Hz, –*CH*CH_3), 5.32 (s, 5H, Cp–*H*$_5$), 6.02–6.19 (m, 5H, Ar–*H*$_5$). Anal. Calcd. for $C_{14}H_{17}F_6OPRu$: C, 37.59; H, 3.83; N, 0.00. Found: C, 37.73; H, 3.71; N, 0.17. FT-IR (ATR, cm^{-1}): 3125 (C–H), 3002 (C–H), 1530 (Ar, C–C) 1457, 1380, 1156 (C–O–C), 1009, 819, 773 (P–F), 555. The corresponding racemate (*rac*-[**1**]PF_6) was synthesized using the same procedure using a racemic ligand (pale yellow crystals, yield 75%).

Preparation of $[Ru(C_5H_5)((S)\text{-}C_6H_5CHCH_3OCH_3)]CB_{11}H_{12}$ ((*S*)-[1]$CB_{11}H_{12}$)

(*S*)-[**1**]PF_6 (220.1 mg, 0.492 mmol) was dissolved in a mixture of acetonitrile (2 mL) and MeOH (20 mL) and charged into a column of anion exchange resin (Dowex 1X8, chloride form). MeOH (100 mL) was used as the eluent to obtain (*S*)-[**1**]Cl. The solution was concentrated and passed through the anion-exchange column again to obtain (*S*)-[**1**]Cl in a solid form almost quantitatively. The disappearance of the PF_6 anion was confirmed in the ^{19}F NMR spectra ($CDCl_3$). An aqueous solution (0.8 mL) of $CsCB_{11}H_{12}$ (49 mg, 0.16 mmol) was added to an aqueous solution (0.1 mL) of (*S*)-[**1**]Cl (35 mg, 0.10 mmol), and the mixture was stirred for 30 min. The solution was filtered, and the filtrate was evaporated under vacuum. The residue was dissolved in a small amount of dichloromethane and filtered. The slow diffusion of diethyl ether into the filtrate at −6 °C precipitated the desired product, which was collected by filtration and dried under vacuum. Colorless block crystals (20 mg, yield 42%) were obtained. ^{1}H NMR (400 MHz, $CDCl_3$): δ = 1.48 (d, 3H, *J* = 6.4 Hz, –CH*CH*$_3$), 1.73–2.54 (br, 12H, carborane–*H*) 3.47 (s, 3H, –O*CH*$_3$), 4.18 (q, 1H, *J* = 6.49 Hz, –*CH*CH_3), 5.38 (s, 5H, Cp–*H*$_5$), 6.10–6.27 (m, 5H, Ar–*H*$_5$). Anal. Calcd. for $C_{15}H_{29}B_{11}ORu$: C, 40.45; H, 6.56; N, 0.00. Found: C, 39.90; H, 6.36; N, 0.00. FT-IR (ATR, cm^{-1}): 3110 (C–H), 2980 (C–H), 2520 (B–H), 1528 (Ar, C–C), 1415, 1150 (C–O–C), 1089, 1064, 1046, 1021, 1001, 866, 846, 716. The corresponding racemate (*rac*-[**1**]$CB_{11}H_{12}$) was synthesized using the same procedure using *rac*-[**1**]Cl instead of (*S*)-[**1**]Cl (colorless block crystals, yield 62%).

Preparation of $[Ru(C_5H_5)((S)\text{-}C_6H_5CHCH_3OCH_3)]CF_3BF_3$ ((*S*)-[1]CF_3BF_3)

An aqueous solution (0.5 mL) of KCF_3BF_3 (197 mg, 1.12 mmol) was added to an aqueous solution (0.5 mL) of (*S*)-[**1**]Cl (177 mg, 0.524 mmol) and stirred for 1 h. The resulting suspension was extracted several times with dichloromethane. The organic layer was dried over anhydrous $MgSO_4$, and the solvent was evaporated under reduced pressure. The residue was washed with toluene, and its solution in acetonitrile was passed through a short column of alumina using acetonitrile as the eluent. After the evaporation of the solvent from the eluted fraction, the product was dried under vacuum at ambient temperature for 2 h and subsequently at 60 °C for 3 h. Pale brown solids (117 mg, yield 50 %) were obtained. ^{1}H NMR (400 MHz, $CDCl_3$): δ = 1.42 (d, 3H, *J* = 6.4 Hz, –CH*CH*$_3$), 3.40 (s, 3H, –O*CH*$_3$), 4.16 (q, 1H, *J* = 6.44 Hz, –*CH*CH_3), 5.38 (s, 5H, Cp–*H*$_5$), 6.02–6.19 (m, 5H, Ar–*H*$_5$). Anal. Calcd. for $C_{15}H_{17}BF_6OPRu$: C, 41.02; H, 3.90; N, 0.00. Found: C, 40.76; H, 3.86; N, 0.00. FT-IR (ATR, cm^{-1}): 3122 (C–H), 1526 (Ar, C–C) 1456, 1417, 1379 (C–F), 1151 (C–O–C), 1044, 1006, 975, 950, 848, 826, 725, 633. The corresponding racemate (*rac*-[**1**]CF_3BF_3) was synthesized using the same procedure using *rac*-[**1**]Cl instead of (*S*)-[**1**]Cl (yellow liquid, yield 76%).

Preparation of $[Ru(C_5H_5)((S)\text{-}C_6H_5CHCH_3OCH_3)]$CPFSA ((*S*)-[1]CPFSA)

An aqueous solution (4 mL) of LiCPFSA (36 mg, 0.12 mmol) was added to a dichloromethane solution (4 mL) of (*S*)-[**1**]Cl (23 mg, 0.068 mmol), and the mixture was stirred for 2 h. The resulting suspension was extracted several times with dichloromethane. The solvent was evaporated under reduced pressure and dried under vacuum. The anion-exchange procedure was performed again using the same procedure. The evaporation of the solvent from the eluted fraction gave an oil, which was subsequently dissolved in dichloromethane (4 mL). The solution was washed three times with water, and the organic layer was dried over anhydrous $MgSO_4$. The solution was passed through a short column of alumina using dichloromethane as the eluent to remove impurities, after which the desired product was eluted with acetonitrile. The solvent was evaporated from the eluted fraction under reduced pressure, and the residue was dried under vacuum at 60 °C for 2 h, after which it was subjected to freeze, pump, and, thaw cycles for the complete removal of the solvents. Yellow liquid (40 mg, yield 95%) was obtained. Anal. Calcd. for $C_{17}H_{17}F_6NO_5RuS_2$: C, 34.34; H, 2.88; N, 2.36. Found: C, 34.74; H, 3.00; N, 2.5. FT-IR (ATR, cm^{-1}): 3110 (C–H), 2926 (C–H), 1530 (Ar, C–C), 1417, 1456, 1352 (C–F), 1156 (C–O–C), 1088 (S=O), 1036 (S=O), 994, 848, 796, 603. ^{1}H NMR (400 MHz, $CDCl_3$): δ = 1.47 (d, 3H, *J* = 6.4 Hz, –CH*CH*$_3$), 3.45 (s, 3H, –O*CH*$_3$), 4.75 (q, 1H, *J* = 6.44 Hz, –*CH*CH_3), 5.39 (s, 5H, Cp–*H*$_5$), 6.12–6.32 (m, 5H, Ar–*H*$_5$). ^{19}F NMR (400 MHz, $CDCl_3$): δ = −119.3, −126.0. The corresponding racemate (*rac*-[**1**]CPFSA) was synthesized using the same procedure using *rac*-[**1**]Cl instead of (*S*)-[**1**]Cl (yellow liquid, yield 80%).

X-ray crystallography

Single-crystal XRD data were collected using a Bruker APEX II Ultra CCD diffractometer with MoKα radiation (λ = 0.71073 Å). The structures were determined by the direct method using SHELXL.[52] Single crystals of *rac*-[**1**]$CB_{11}H_{12}$ and (*S*)-[**1**]PF_6 were produced by the slow diffusion of diethyl ether into a dichloromethane solution at −6 °C and the slow cooling of the solution in dichloromethane–diethyl ether at −40 °C, respectively. The α- and β-polymorphs of *rac*-[**1**]$CB_{11}H_{12}$ were platelet and block crystals, respectively. Their crystallographic parameters are listed in Table S1 (ESI†).

Acknowledgements

This work was supported financially by KAKENHI (20H02756) from the Japan Society for the Promotion of Science (JSPS).

Notes and references

1 S. d'Agostino, L. Fornasari and D. Braga, *Cryst. Growth Des.*, 2019, **19**, 6266–6273.
2 W. A. Henderson, V. G. Young, S. Passerini, P. C. Trulove and H. C. De Long, *Chem. Mater.*, 2006, **18**, 934–938.
3 K. Matsumoto, U. Harinaga, R. Tanaka, A. Koyama, R. Hagiwara and K. Tsunashima, *Phys. Chem. Chem. Phys.*, 2014, **16**, 23616–23626.
4 Y. Yamada, E. Kashimoto and H. Honda, *Bull. Chem. Soc. Jpn.*, 2019, **92**, 1289–1298.
5 J. M. Pringle, P. C. Howlett, D. R. MacFarlane and M. Forsyth, *J. Mater. Chem.*, 2010, **20**, 2056–2062.
6 H. Zhu, D. R. MacFarlane, J. M. Pringle and M. Forsyth, *Trends Chem*., 2019, **1**, 126–140.
7 J. Harada, Y. Kawamura, Y. Takahashi, Y. Uemura, T. Hasegawa, H. Taniguchi and K. Maruyama, *J. Am. Chem. Soc.*, 2019, **141**, 9349–9357.
8 Z.-B. Zhou and H. Matsumoto, *Electrochem. Commun.*, 2007, **9**, 1017–1022.
9 P.-F. Li, Y.-Y Tang, Z.-X. Wang, H.-Y. Ye, Y.-M. You and R.-G. Xiong, *Nat. Commun.*, 2016, **7**, 13635.
10 M. Yoshizawa-Fujita, E. Kishi, M. Suematsu, T. Takekawa and M. Rikukawa, *Chem. Lett*., 2014, **43**, 1909–1911.
11 M. Kar, K. Matuszek and D. R. MacFarlane, *Ionic liquids* in *Kirk-Othmer Encyclopedia of Chemical Technology*, John Wiley & Sons, Inc., Hoboken, 2019.
12 H. Kimata and T. Mochida, *Cryst. Growth Des*., 2018, **18**, 7562–7569.
13 T. Mochida, Y. Funasako, M. Ishida, S. Saruta, T. Kosone and T. Kitazawa, *Chem. Eur. J*., 2016, **22**, 15725–15732.
14 T. Mochida, Y. Funasako, T. Inagaki, M.-J. Li, K. Asahara and D. Kuwahara, *Chem. Eur. J.*, 2013, **19**, 6257–6264.
15 T. Mochida, M. Ishida, T. Tominaga, K. Takahashi, T. Sakurai and H. Ohta, *Phys. Chem. Chem. Phys*., 2018, **20**, 3019–3028.
16 H. Kimata, T. Sakurai, H. Ohta and T. Mochida, *ChemistrySelect*, 2019, **4**, 1410–1415.
17 T. Inagaki, T. Mochida, M. Takahashi, C. Kanadani, T. Saito and D. Kuwahara, *Chem*. *Eur*. *J*., 2012, **18**, 6795–6804.
18 Y. Funasako, S. Mori and T. Mochida, *Chem*. *Commun*., 2016, **52**, 6277–6279.
19 R. Sumitani, H. Yoshikawa and T. Mochida, *Chem. Commun.*, 2020, **56**, 6189–6192.
20 Y. Funasako, T. Mochida, T. Inagaki, T. Sakurai, H. Ohta, K. Furukawa and T. Nakamura, *Chem*. *Commun*., 2011, **47**, 4475–4477.
21 T. Ueda, T. Tominaga, T. Mochida, K. Takahashi and S. Kimura, *Chem. Eur. J.*, 2018, **24**, 9490–9493.
22 R. J. Webb, M. D. Lowery, Y. Shiomi, M. Sorai, R. J. Wittebort, and D. N. Hendrickson, *Inorg. Chem.*, 1992, **31**, 5211–5219.
23 D. Braga, F. Grepioni and G. R. Desiraju, *Chem. Rev.*, 1998, **98**, 1375–1406.
24 T. Tominaga, T. Ueda and T. Mochida, *Phys. Chem. Chem. Phys.*, 2017, **19**, 4352–4359.
25 D. Al-Masri, R. Yunis, A. F. Hollenkamp, C. M. Doherty and J. M. Pringle, *Phys. Chem. Chem. Phys.*, 2020, **22**, 18102–18113.
26 J. Jacques, A. Collet and S. H. Wilen, *Enantiomers, Racemates and Resolution*, Krieger Pub. Co., Malabar, Florida, 1991.
27 E. L. Eliel, S. H. Wilen and L. N. Mander, *Stereochemistry of Organic Compounds*, Wiley-Interscience, New York, 1994.
28 A. A. Bredikhin, Z. A. Bredikhina and D. V. Zakharychev, *Mendeleev Commun*., 2012, **22**, 171–180.
29 C. Brandel, S. Petit, Y. Cartigny and G. Coquerel, *Curr. Pharm. Des.*, 2016, **22**, 4929–4941.
30 B. Chion, J. Lajzerowicz, D. Bordeaux, A. Collet and J. Jacques, *J. Phys. Chem*., 1978, **82**, 2682–2688.
31 T. Payagala and D. W. Armstrong, *Chirality*, 2012, **24**, 17–53.
32 J. Flieger, J. Feder-Kubis and M. Tatarczak-Michalewska, *Int. J. Mol. Sci.*, 2020, **21**, 4253.
33 S. Payra, A. Saha and S. Banerjee, *Curr. Organocatal.*, 2017, **4**, 4–32.
34 D. Wu, P. Cai, X. Zhao, Y. Kong and Y. Pan, *J. Sep. Sci.*, 2018, **41**, 373–384.
35 Y. Miura, T. Mochida, S. Motodate and K. Kato, *Polyhedron*, 2016, **113**, 1–4.
36 T. Higashi, T. Ueda and T. Mochida, *Phys. Chem. Chem. Phys.*, 2016, **18**, 10041–10048.
37 M. Matsuki, T. Yamada, S. Dekura, H. Kitagawa and N. Kimizuka, *Chem. Lett*., 2018, **47**, 497–499.
38 M. Matsuki, T. Yamada, N. Yasuda, S. Dekura, H. Kitagawa and N. Kimizuka, *J. Am. Chem. Soc.*, 2018, **140**, 291–297.
39 I. B. Rietveld, M. Barrio, N. Veglio, P. Espeau, J. L. Tamarit and R. Céolin, *Thermochim. Acta*, 2010, **511**, 43–50.
40 H. Kimata, R. Sumitani and T. Mochida, *Chem*. *Lett*., 2019, **48**, 859–862.
41 J. Timmermans, *J. Phys. Chem. Solids*, 1961, **18**, 1–8.
42 J. N. Sherwood, The Plastically Crystalline State: Orientationally Disordered Crystals, John Wiley & Sons, Chichester, UK, 1979.
43 C. P. Brock, W. B. Schweizer and J. D. Dunitz, *J. Am. Chem. Soc*., 1991, **113**, 9811–9820.
44 O. Wallach, *Liebigs Ann. Chem*., 1895, **286**, 90–143.
45 A. L. Rohl and D. M. P. Mingos, *Inorg. Chim. Acta*, 1993, **212**, 5–13.
46 P. Atkins, T. Overton, J. Rourke, M. Weller, F. Armstrong and M. Hagerman, *Shriver and Atkins' Inorganic Chemistry*, 5th ed., Oxford University Press, Oxford, 2010.
47 D. Turnbull and M. H. Cohen, *Crystallization Kinetics and Glass Formation* in *Modern Aspect of the Vitreous State*, ed. J. D. MacKenzie, Butterworth & Co. Publishers Ltd., London, vol. 1, 1960.
48 O. Yamamuro, Y. Minamimoto, Y. Inamura, S. Hayashi and H. Hamaguchi, *Chem. Phys. Lett.*, 2006, **423**, 371–375.
49 M. Leclercq, A. Collet and J. Jacques, *Tetrahedron*, 1976, **32**, 821–828.
50 B. M. Trost and C. M. Older, *Organometallics*, 2002, **21**, 2544–2546.
51 S. H. Lee, I. S. Kim, Q. R. Li, G. R. Dong, L. S. Jeong and Y. H. Jung, *J. Org. Chem*., 2011, **76**, 10011–10019.
52 G. M. Sheldrick, *Acta Crystallogr.*, 2008, A**64**, 112–122.

TOC

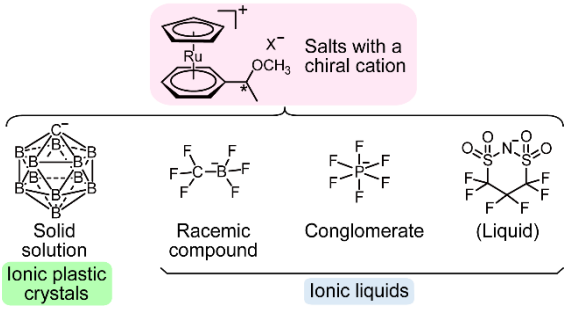

Salts of a chiral ruthenium sandwich complex with various anions were synthesized and their phase diagrams were investigated.

Supporting Information

Thermal Properties, Crystal Structures, and Phase Diagrams of Ionic Plastic Crystals and Ionic Liquids Containing a Chiral Cationic Sandwich Complex

Tomoyuki Mochida,*[a,b] Ryo Sumitani[a], and Tomoaki Yamazoe[a]

[a]*Department of Chemistry, Graduate School of Science, Kobe University, 1-1 Rokkodai, Nada, Kobe, Hyogo 657-8501, Japan*
E-mail: tmochida@platinum.kobe-u.ac.jp
[b]*Center for Membrane Technology, Kobe University, 1-1 Rokkodai, Nada, Kobe, Hyogo 657-8501, Japan*

Content

Fig. S1. DSC traces of [**1**]CPFSA (100% ee, 50% ee, and 0% ee).

Fig. S2. DSC traces of [**1**]$CB_{11}H_{12}$ (100% ee, 51% ee, and 0% ee).

Fig. S3. PXRD patterns of (a) (*S*)- and (b) *rac*-[**1**]$CB_{11}H_{12}$ at 20 and 80 °C (MoKα radiation).

Fig. S4. PXRD patterns: (a) (*S*)-[**1**]CF_3BF_3 (20 °C) and *rac*-[**1**]CF_3BF_3 (0, 10 °C). (b) (*S*)-[**1**]PF_6 (20 °C), *rac*-[**1**]PF_6 (20 °C), and (*S*)-[**1**]PF_6 (simulated, MoKα radiation).

Fig. S5. ^{1}H NMR spectrum of (*S*)-[**1**]PF_6 (400 MHz, Solvent: $CDCl_3$).

Table S1. Crystallographic parameters.

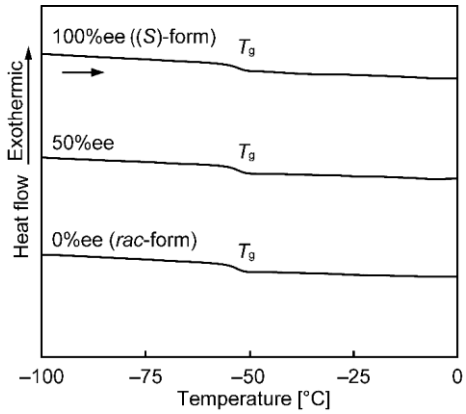

Fig. S1. DSC traces of [**1**]CPFSA (100% ee, 50% ee, and 0% ee).

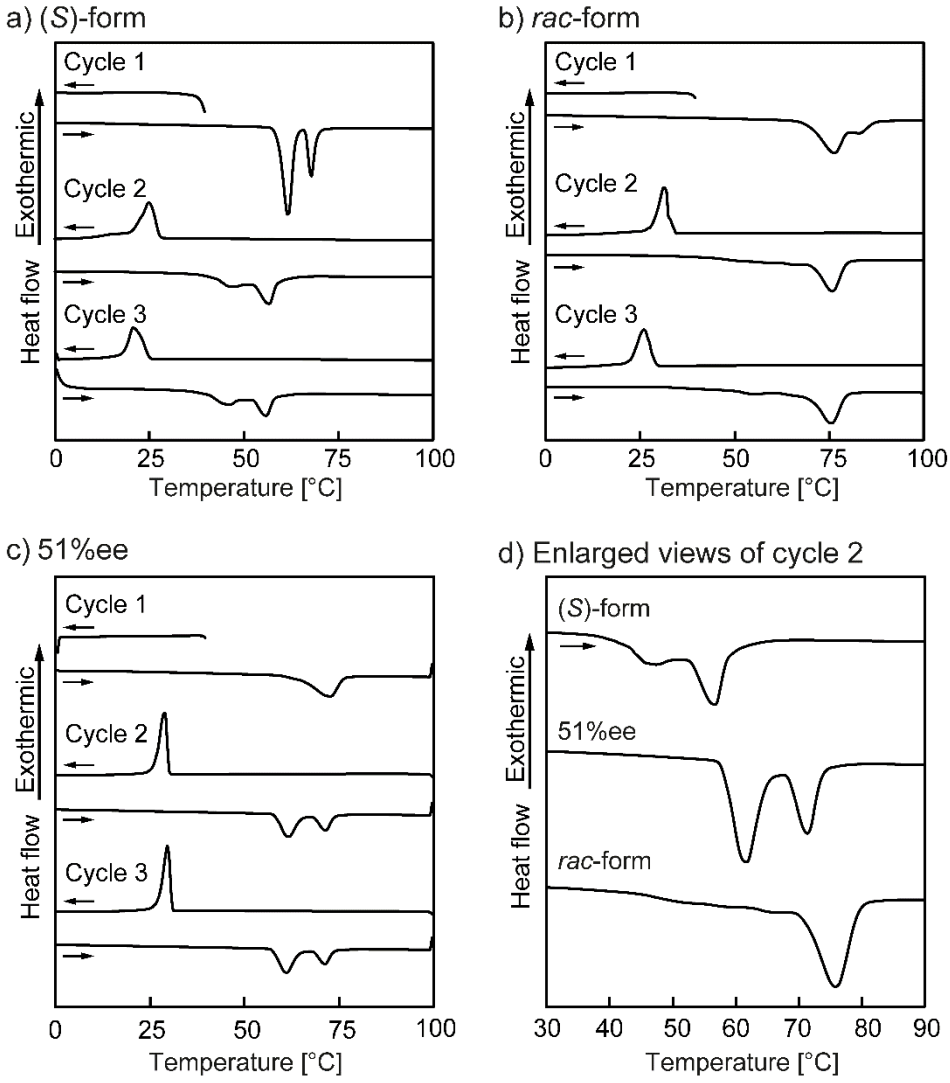

Fig. S2. DSC traces of [**1**]$CB_{11}H_{12}$ (100% ee, 51% ee, and 0% ee).

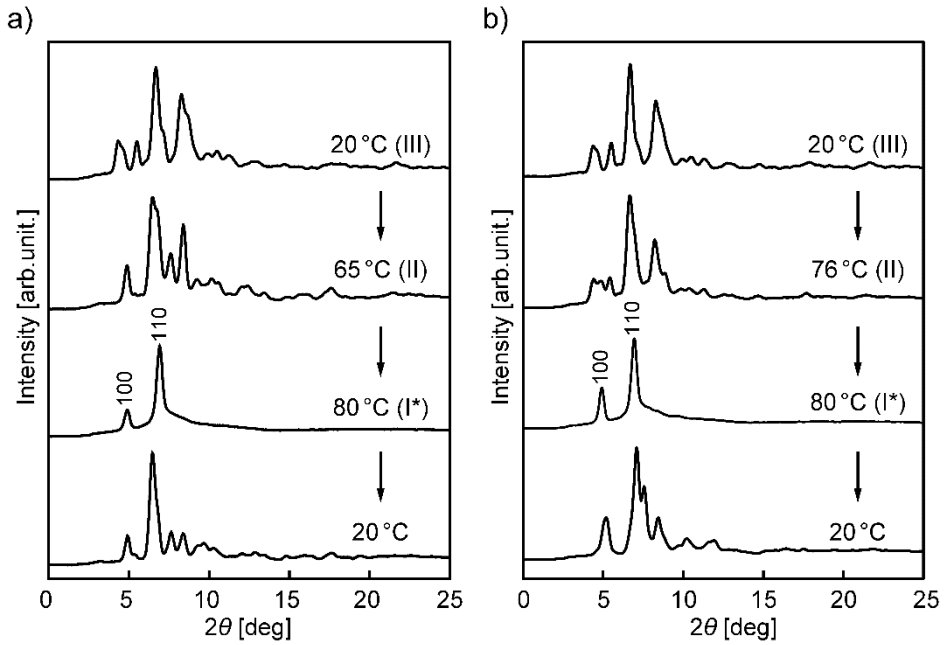

Fig. S3. PXRD patterns of (a) (*S*)- and (b) *rac*-[**1**]$CB_{11}H_{12}$ at 20 and 80 °C (MoKα radiation).

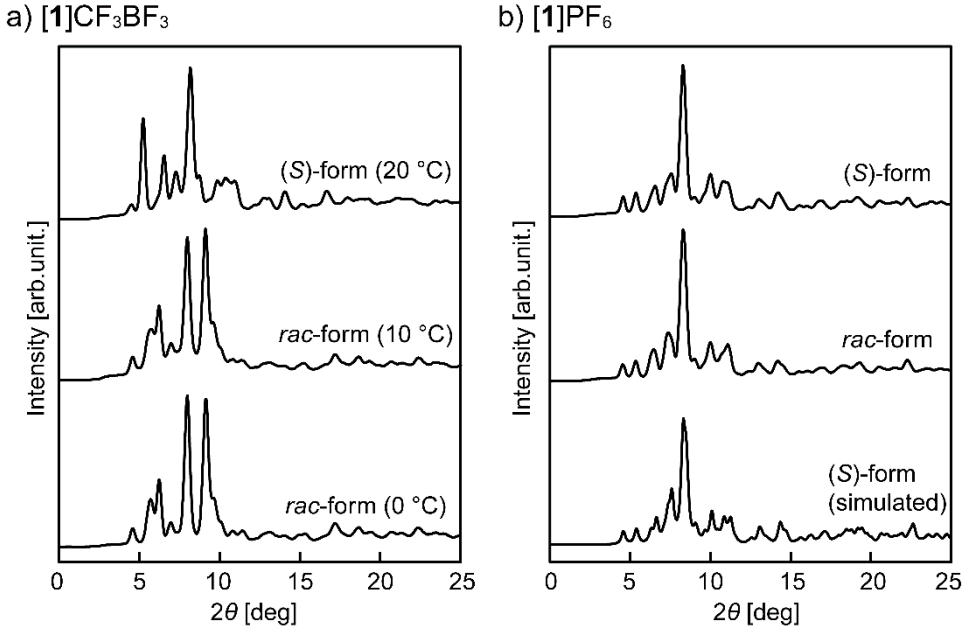

Fig. S4. PXRD patterns: (a) (*S*)-[**1**]CF_3BF_3 (20 °C) and *rac*-[**1**]CF_3BF_3 (10, 0 °C). (b) (*S*)-[**1**]PF_6 (20 °C), *rac*-[**1**]PF_6 (20 °C), and (*S*)-[**1**]PF_6 (simulated, MoK*α* radiation).

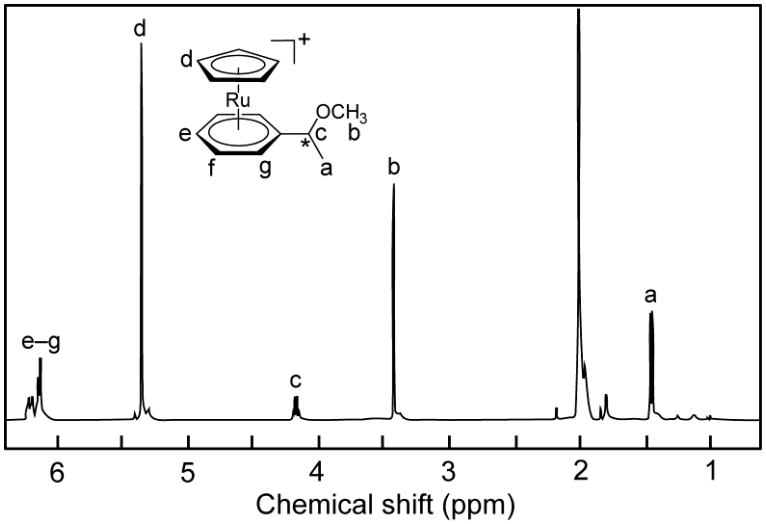

Fig. S5. ^{1}H NMR spectrum of (*S*)-[**1**]PF_6 (400 MHz, Solvent: $CDCl_3$).

Table S1. Crystallographic parameters of *S*-[**1**]PF_6 and *rac*-[**1**]$CB_{11}H_{12}$.

	S-[**1**]PF_6	*rac*-α-[**1**]$CB_{11}H_{12}$	*rac*-β-[**1**]$CB_{11}H_{12}$
Empirical formula	$C_{14}H_{17}F_6OPRu$	$C_{15}H_{29}B_{11}ORu$	$C_{15}H_{29}B_{11}ORu$
Formula weight	447.31	445.36	445.36
Crystal system	Orthorhombic	monoclinic	triclinic
Space group	$P2_12_12_1$	$P2_1/c$	P–1
a [Å]	9.5873(6)	9.590(2)	8.7042(10)
b [Å]	12.2766(8)	22.809(5)	10.1448(12)
c [Å]	12.9471(8)	9.636(2)	12.0722(14)
α [°]	90	90	99.0460(10)
β [°]	90	94.756(3)	95.8930(10)
γ [°]	90	90	96.4770(10)
V [Å^3]	1523.87(17)	2100.5(9)	1038.1(2)
Z	4	4	2
ρ_{calcd} [g cm^{-3}]	1.950	1.408	1.425
F(000)	888	904	452
Temperature [K]	90	90	90
Reflns collected	8801	11884	5300
Independent reflns	3494	4862	3865
Parameters	210	285	259
R_{int}	0.0197	0.0514	0.0157
R_1[a], R_w[b] ($I > 2\sigma$)	0.0144, 0.0364	0.0527, 0.0963	0.0201, 0.0532
R_1[a], R_w[b] (all data)	0.0145, 0.0364	0.0852, 0.1059	0.0203, 0.0533
Goodness of fit	1.147	1.102	1.089
$\Delta\rho_{max,min}$ [e Å^{-3}]	0.301, –0.785	1.090, –1.354	0.330, –0.557
Flack parameter	0.037	–	–

[a] $R_1 = \Sigma||F_o| - |F_c|| / \Sigma|F_o|$. [b] $R_w = [\Sigma w (F_o^2 - F_c^2)^2 / \Sigma w (F_o^2)^2]^{1/2}$